NMR Solution Structure of Type II Human Cellular Retinoic Acid Binding Protein: Implications for Ligand Binding[†,‡]

Lincong Wang,[§] Yue Li,[§] Frits Abildgaard,[||] John L. Markley,[||] and Honggao Yan*[,§]

Department of Biochemistry, Michigan State University, East Lansing, Michigan 48824, and Department of Biochemistry, University of Wisconsin−Madison, 420 Henry Mall, Madison, Wisconsin 53706

Received April 20, 1998; Revised Manuscript Received July 21, 1998

ABSTRACT: The structure of human apo-cellular retinoic acid binding protein II (apo-CRABPII) in solution at pH 7.3 has been determined by NMR spectroscopy. The sequential assignments of the ^{1}H, ^{13}C, and ^{15}N resonances of apo-CRABPII were established by multinuclear, multidimensional NMR spectroscopy. The solution structure of apo-CRABPII was derived from 2382 experimental NMR restraints using a hybrid distance geometry-simulated annealing protocol. The root-mean-square deviation of the ensemble of 25 refined conformers that represent the structure from the mean coordinate set derived from them was 0.54 ± 0.18 and 0.92 ± 0.20 Å for the backbone atoms and all heavy atoms, respectively, of all residues except Ala32−Pro39 and Thr57−Glu62, which are in disordered regions. The solution structure of apo-CRABPII is similar to the crystal structure of holo-CRABPII [Kleywegt, G. J., Bergfors, T., Senn, H., Le Motte, P., Gsell, B., Shudo, K., and Jones, T. A. (1994) *Structure 2*, 1241−1258] except the ligand entrance, which is sufficiently enlarged in the apoprotein to be readily accessible to retinoic acid. The enlargement of the ligand entrance of apo-CRABPII relative to that of holo-CRABPII is due mainly to a concerted conformational change in three structural elements, namely, the second helix, the βC−βD loop, and the βE−βF loop. Furthermore, the ligand-binding pocket of apo-CRABPII showed evidence of dynamic disorder; among the 21 residues that constitute this pocket, 16 residues had weak or no detectable cross-peaks in the two-dimensional ^{1}H−^{15}N HSQC spectrum recorded under conditions of minimal water saturation or dephasing. Apo-CRABPII is largely monomeric in solution, with no evidence for the dimeric structure shown in the crystal structure of apo-CRABPI which was suggested to be a prerequisite for ligand entry [Thompson, J. R., Bratt, J. M., and Banaszak, L. J. (1995) *J. Mol. Biol. 252*, 433−446]. Thus, the widening of the ligand entrance required for entry of retinoic acid appears to be a property of monomeric apo-CRABPII.

Retinoic acid (RA[1]), a hormonally active metabolite of vitamin A, has profound effects on cell growth, differentiation, and morphogenesis (*1*). Particularly, it plays important roles in embryonic development and maintenance of normal epithelial tissues. Either RA deficiency or excess results in developmental defects. The plethora of biological effects of RA and other retinoids are believed to be mediated by various nuclear RA receptors (RARs and RXRs), all of which are RA-activated transcriptional factors that regulate the expression of target genes (*2*). RA and synthetic retinoids have been used for treatment of skin disorders, epithelial malignancies, such as skin cancer and cervical cancer, and hematological malignancies, such as acute promyelocytic leukemia.

In addition to nuclear RA receptors, two types of cellular retinoic acid binding proteins (CRABPI and CRABPII) are also implicated in RA signal transduction (*3*). However, their physiological functions are still being debated. It is thought that CRABPs may protect cells from the detrimental effects of RA by preventing it from being incorporated into membranes. Indeed, in the tissues that express CRABPs, RA is found predominately in protein-bound forms. More recently, a model for RA metabolism with CRABPI playing more active roles has been proposed (*1*). On the other hand, "knockout" mice deficient in CRABPII or in both CRABPI and CRABPII appeared to be normal, except for some minor defects in limb development (*2*, *3*).

[†] This work was supported by funds from the REF Center of Protein Structure and Design and the Cancer Center at Michigan State University and the NIH (Grant GM51901). This study made use of a Varian INOVA-600 NMR spectrometer at Michigan State University funded in part by NSF Grant BIR9512253 and the National Magnetic Resonance Facility at Madison with operating costs subsidized by NIH Grant RR02301 and equipment funded by the University of Wisconsin, NSF, NIH, and USDA.

[‡] The ensemble of NMR structures and constraints have been deposited at the Protein Data Bank (http://www.pdb.bnl.gov) under PDB code 1blr.

* To whom correspondence should be addressed at the Department of Biochemistry, Michigan State University, East Lansing, MI 48824. Telephone: (517) 353-8786. Fax: (517) 353-9334. E-mail: yanh@pilot.msu.edu.

[§] Michigan State University.

[||] University of Wisconsin−Madison.

[1] Abbreviations: 2D, two-dimensional; 3D, three-dimensional; CRABP, cellular retinoic acid binding protein; CRBP, cellular retinol binding protein; DQF-COSY, double-quantum filtered correlation spectroscopy; HSQC, heteronuclear single-quantum coherence; iLBP, intracellular lipid binding protein; NMR, nuclear magnetic resonance; NOE, nuclear Overhauser effect; NOESY, nuclear Overhauser effect spectroscopy; RA, all-*trans*-retinoic acid; RAR, retinoic acid receptor; rmsd, root-mean-square deviation; RXR, retinoid X receptor; TOCSY, total correlation spectroscopy.

S0006-2960(98)00892-7 CCC: $15.00
Published on Web 08/25/1998

The two CRABPs are highly homologous with 74% sequence identity between human CRABPI and CRABPII (*4*). Furthermore, they are extremely conserved between species. For example, human CRABPI differs by only one residue from those of rat, mouse, and cow, and the latter are all identical. It has been thought that the high degree of sequence identity is required not just for conservation of structure and ligand specificity but for maintaining interactions with other proteins such as RA-metabolizing enzymes (*5*). Although the two proteins have similar specificities and affinities for RA (*6*−*8*), they differ in spatial and temporal expression patterns and regulation, suggesting that CRABPI and CRABPII may play distinct important cellular functions. It has been shown that production of RA is correlated with the expression of CRABPII but not CRABPI (*9*). Overexpression of CRABPII enhances cellular response to RA in breast cancer cells (*10*), but overexpression of CRABPI decreases the biological potency of RA in F9 teratocarcinoma cells (*11*).

CRABPs belong to the family of intracellular lipid binding proteins (iLBPs) that bind small hydrophobic molecules such as retinoids and fatty acids (*12*). This family of proteins is characterized by a low level of identity (∼20%) in its sequence and a high level of similarity in its folding. All known structures consist of a helix−turn−helix motif and two nearly orthogonal five-stranded β-sheets. A flattened β-barrel formed by the two β-sheets serves as a deep ligand-binding pocket with the helix−turn−helix motif at the entrance. One of the key questions concerning the family of iLBPs is how the ligands move in and out of their respective binding pockets, since they are encapsulated by the β-sheets and the helix−turn−helix motif in most cases.

The crystal structures of holo-CRABPI and holo-CRABPII (both in complex with all-*trans*-RA) have been determined (*13*). In each structure, RA is buried deeply in the RA-binding pocket, with its carboxyl group interacting with the side chains of two arginines and one tyrosine at the bottom of the pocket. The β-ionone ring which is fixed snugly at the entrance of the RA-binding pocket with only one edge of the ring accessible to the solvent is forced to adopt an unusual cis-like conformation. It appears that RA cannot enter or exit the deep binding pocket in the absence of major conformational changes in the protein. More recently, the crystal structure of apo-CRABPI has been solved (*14*). The ligand entrance of apo-CRABPI is slightly more open than that of holo-CRABPI and thus a bit more accessible to RA. Surprisingly, apo-CRABPI is a dimer in the crystalline state, held together by an intermolecular β-sheet. Dimerization has been suggested to be the mechanism that allows RA to enter or exit the RA-binding pocket and by which CRABPI interacts with RA-metabolizing enzymes such as cytochrome P450s. However, it is unclear whether apo-CRABPI is dimeric in solution. CRABPI has been studied by NMR (*15*), but no solution NMR structure has been reported.

In this paper, we report the solution structure of human apo-CRABPII determined by NMR spectroscopy at pH 7.3. The sequential assignments of the ^{1}H, ^{13}C, and ^{15}N resonances of apo-CRABPII were established by multinuclear, multidimensional NMR experiments. The solution structure of apo-CRABPII was derived from 2382 experimental NMR restraints. The NMR structure is similar to the crystal structure of holo-CRABPII, but significant conformational differences were observed, especially in the ligand entrance region. The structure of holo-CRABPII can be converted to that of apo-CRABPII, which has a greatly enlarged ligand entrance, by concerted movements of the second helix, the βC−βD loop, and the βE−βF loop. Furthermore, the ligand-binding pocket of apo-CRABPII exhibits dynamic disorder in solution. The results suggest that binding of RA induces significant changes in the conformation and dynamics of CRABPII.

EXPERIMENTAL PROCEDURES

Sample Preparation. Unlabeled human CRABPII was overexpressed and purified as previously described (*8*). The same procedure was used for isotopic labeling of CRABPII except for some minor modifications as described in detail below. M9 media were used for the uniform isotopic labeling of CRABPII with $^{15}NH_4Cl$ and [$^{13}C_6$]-D-glucose as the sole nitrogen and carbon sources for ^{15}N- and ^{13}C-labeling, respectively. For ^{15}N-labeling of leucine and valine residues, a rich medium containing [^{15}N]valine or [^{15}N]-leucine was used (*16*). The *Escherichia coli* strain DL49PS pLysS (kindly provided by D. M. LeMaster) was used for the selective isotopic labeling. D_2O samples were prepared by dissolving lyophilized unlabeled CRABPII in PBS buffer [20 mM sodium phosphate and 150 mM sodium chloride in 99.6% D_2O (pD 7.5, uncorrected)]. H_2O samples were prepared by directly concentrating CRABPII fractions eluted with the PBS buffer (pH 7.3) from a gel-filtration column at the final step of the purification procedure (*8*). About 10% D_2O was added to the concentrated protein solutions. The protein concentrations of the NMR samples were ∼2 mM.

NMR Spectroscopy. The 600 MHz NMR spectra were acquired on a Varian INOVA-600 spectrometer, and 500 MHz spectra were acquired on a Bruker DMX-500 spectrometer. The carrier frequencies for various experiments were as follows: ^{1}H, 4.70 ppm; ^{15}N, 119.7 ppm; ^{13}CO, 175 ppm; $^{13}C^{\alpha}$, 54 ppm; and $^{13}C^{\alpha/\beta}$, 43 ppm. Quadrature detection in the nonacquisition dimensions was achieved by the hypercomplex method (*17*) for homonuclear experiments and by the States−TPPI method (*18*) for heteronuclear experiments. The sample temperature was 25 °C.

Homonuclear 2D spectra were recorded for the D_2O samples with the following acquisition times and numbers of complex points: DQF-COSY (*19*, *20*), F_1, 61.0 ms and 512, and F_2, 243.8 ms and 2048 (128 transients); TOCSY (*21*−*23*), F_1, 38.1ms and 320, and F_2, 243.8 ms and 2048 (64 transients); and NOESY (*24*, *25*), F_1, 38.1 ms and 320, and F_2, 243.8 ms and 2048 (64 transients). Two TOCSY spectra were acquired, one with a 30 ms mixing time and one with a 50 ms mixing time. Two NOESY spectra were recorded, one with a 100 ms mixing time and one with a 150 ms mixing time. A SSNOESY (*26*) spectrum was recorded in H_2O with the following acquisition parameters: F_1, 61.0 ms and 512, and F_2, 243.8 ms and 2048 (64 transients, 150 ms mixing time). The homonuclear 2D data were processed with the program VNMR, version 5.2 (Varian Associates). Apodization functions applied to the 2D NOESY and TOCSY data were a Gaussian and minus LB combination in the F_1 dimension and a ∼75° shifted sine-bell function in the F_2 dimension; apodization functions

applied to the 2D DQF-COSY data were an ~30° shifted sine-bell function in both the F_1 and F_2 dimensions. The data sets were zero filled to 4096 × 2048 real points for TOCSY and NOESY or 8192 × 4096 real points for DQF-COSY experiments. In general, a five-order polynomial was applied for baseline correction in the F_2 dimension after Fourier transformation.

Heteronuclear double- and triple-resonance spectra were acquired with the following acquisition times and numbers of complex points: 2D ^{1}H−^{15}N HSQC (*27*, *28*), ^{15}N (F_1), 53.3 ms and 128, and ^{1}H (F_2), 121.9 ms and 1024 (32 transients); 3D ^{1}H−^{15}N NOESY−HSQC (*29*−*31*), ^{1}H (F_1), 33.2 ms and 200, ^{15}N (F_2), 34.0 ms and 68, ^{1}H (F_3), 141.5 ms and 1024 (16 transients, 150 ms mixing time); CT-HNCO (*32*, *33*), ^{15}N (F_1), 16.0 ms and 32, ^{13}CO (F_2), 34.0 ms and 64, ^{1}H (F_3), 127.80 ms and 1024 (16 transients); CT-HNCA (*32*, *33*) and CT-HN(CO)CA (*33*, *34*), ^{15}N (F_1), 16.0 ms and 32, ^{13}C$^\alpha$ (F_2), 10.9 ms and 64, ^{1}H (F_3), 127.80 ms and 1024 (16 transients); HNCACB (*35*, *36*), ^{13}C$^{\alpha/\beta}$ (F_1), 7.1 ms and 64, ^{15}N (F_2), 15.2 ms and 32, ^{1}H (F_3), 128.0 ms and 1024 (32 transients); CBCA(CO)NH (*36*, *37*), ^{13}C$^{\alpha/\beta}$ (F_1), 6.4 ms and 64, ^{15}N (F_2), 16.0 ms and 32, ^{1}H (F_3), 127.80 ms and 1024 (32 transients); C(CO)NH (*36*, *38*), ^{13}C (F_1), 9.7 ms and 96, ^{15}N (F_2), 15.2 ms and 32, ^{1}H (F_3), 128.0 ms and 1024 (32 transients); H(CCO)NH (*36*, *38*), ^{1}H (F_1), 15.9 ms and 128, ^{15}N (F_2), 25.0 ms and 50, ^{1}H (F_3), 127.80 ms and 1024 (32 transients); HCCH−TOCSY (*39*, *40*), ^{1}H (F_1), 35.8 ms and 128, ^{13}C (F_2), 10.5 ms and 75, ^{1}H (F_3), 127.80 ms and 1024 (16 transients, 16 ms mixing time). A low-power GARP-I sequence (*41*) was applied for ^{15}N broad-band decoupling during the data acquisition. ^{1}H broad-band decoupling in the CT-HNCO, CT-HNCA, CT-HN(CO)CA, C(CO)NH, and H(CCO)NH experiments was achieved by the DIPSI-2 sequence (*42*), and in the CBCA(CO)NH experiment by the WALTZ-16 sequence (*43*). CO decoupling during $C^{\alpha/\beta}$ chemical shift evolution and C^α−^{15}N scalar coupling periods in the HNCACB experiment and $^{13}C^\alpha$ decoupling during the constant time t_2 (^{15}N) in the CBCA(CO)NH experiment were accomplished by applying a SEDUCE-1 ^{13}C homonuclear sequence (*44*). The ^{13}C isotropic mixings in the HCCH-TOCSY, H(CCO)NH, and C(CO)NH experiments were accomplished by the DIPSI-3 sequence (*42*). The HSQC, HNCACB, and C(CO)NH spectra were acquired on the INOVA-600 spectrometer and processed with the program VNMR, version 5.3 (Varian Associates). All the other spectra were acquired on the DMX500 spectrometer and processed with Felix 95 (Biosym Technologies). Briefly, the first points of both F_1 and F_2 dimensions were calculated by linear predictions. The data size in the F_1 or F_2 dimension was extended by backward−forward linear prediction (*45*). Solvent suppression was improved by convolution of time domain data (*46*). Shifted sine-bell and single zero-filling functions were generally applied before Fourier transformation in each dimension.

Derivation of Structural Restraints. Approximate interproton distance restraints were derived from the NOE data. NOE cross-peaks between aliphatic protons were picked from the homonuclear 2D NOESY spectrum with the mixing time of 100 ms using the program VNMR, version 5.2. NOE cross-peaks involving amide protons were picked from the 3D ^{1}H−^{15}N NOESY−HSQC data with the mixing time of 150 ms using the program Felix 95, except for those of Ile9, Ile10, Ile63, Arg132, Val133, and Tyr134, which were picked from the 2D homonuclear NOESY spectrum. The integrated peak volumes were converted into approximate interproton distances by normalizing them against the calibrated volumes of NOE peaks between backbone protons within the identified β-sheet regions. The upper limits of the interproton distances were calibrated according to the equation $V_a = V_b(r_b/r_a)^6$, where V_a and V_b were the volumes and r_a and r_b the distances. The distance bounds were then set to 1.8−2.7 Å (1.8−2.9 Å for NOE cross-peaks involving amide protons), 1.8−3.3 Å (1.8−3.5 Å for NOE cross-peaks involving amide protons), and 1.8−5.0 Å corresponding to strong, medium, and weak NOEs, respectively. Pseudoatom corrections were made for nonstereospecifically assigned methylene and methyl resonances (*47*). An additional 0.5 Å was added to the upper bounds for methyl protons.

Protein backbone hydrogen bonds were derived from patterns of cross-peaks remaining in the fingerprint regions of the homonuclear 2D TOCSY and NOESY spectra recorded in D_2O. Hydrogen bond restraints were set to 2.0 ± 0.5 Å for H^N···O and 3.0 ± 0.3 Å for N···O distances.

Structure Calculation. The structures were calculated with a hybrid distance geometry-simulated annealing (DGSA) protocol (*48*) using the program X-PLOR (version 3.1) (*49*) on an SGI Indigo II workstation. A square-well potential function with a force constant of 50 kcal mol^{-1} Å^{-2} was applied for the distance restraints. The X-PLOR f_{repel} function was used to simulate van der Waals interactions, with atomic radii set to 80% of their CHARMM values (*50*). Hydrogen bond restraints within the regions of regular secondary structures were introduced at a later stage of structural refinement. A total of 70 structures were generated using this protocol. The structures were inspected by the programs QUANTA96 (Molecular Simulations) and InsightII (Biosym Technologies) and analyzed by PROCHECK-NMR (version 3.4.4) (*51*, *52*). An iterative strategy was used for the structure refinement. In each round of structure refinement, newly computed NMR structures were employed to assign more NOE restraints, to correct wrong assignments, and to loosen the NOE distance bounds if spectral overlapping was deduced. Then another round of structure refinement was carried out with the modified NMR restraints. After several rounds of such refinement, an ensemble of 25 structures was selected, from a total of 55 converged structures, according to their best fit to the experimental NMR restraints and the low values of their total energies.

RESULTS AND DISCUSSION

Sequential Resonance Assignment. HNCACB and CBCA(CO)NH spectra were first analyzed to obtain sequential connectivities. Representative results are shown in Figure 1. About 100 residues with relatively strong peaks in the 2D ^{1}H−^{15}N HSQC spectrum (Figure 2) could be easily linked on the basis of these two sets of data. These residues were then sequentially assigned by the combined analyses of the 3D C(CO)NH, H(CCO)NH, HCCH−TOCSY, and homonuclear 2D TOCSY spectra.

The majority of the remaining residues had weak or no detectable peaks in the ^{1}H−^{15}N HSQC spectrum, even with minimal water perturbation. Because these residues also had weak or no detectable cross-peaks in the triple-resonance

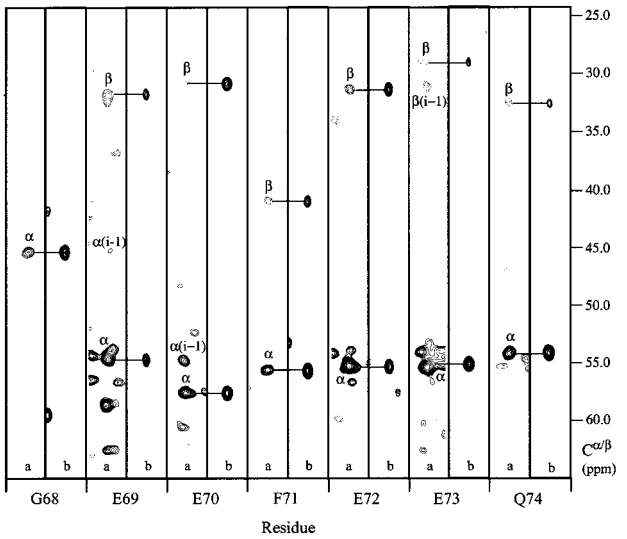

FIGURE 1: Strips of the HNCACB (a) and CBCA(CO)NH (b) spectra showing the sequential connectivities for residues Gly68−Gln74. Both interresidue and intraresidue peaks in the HNCACB strips (a) are labeled. The dotted lines indicate negative peaks.

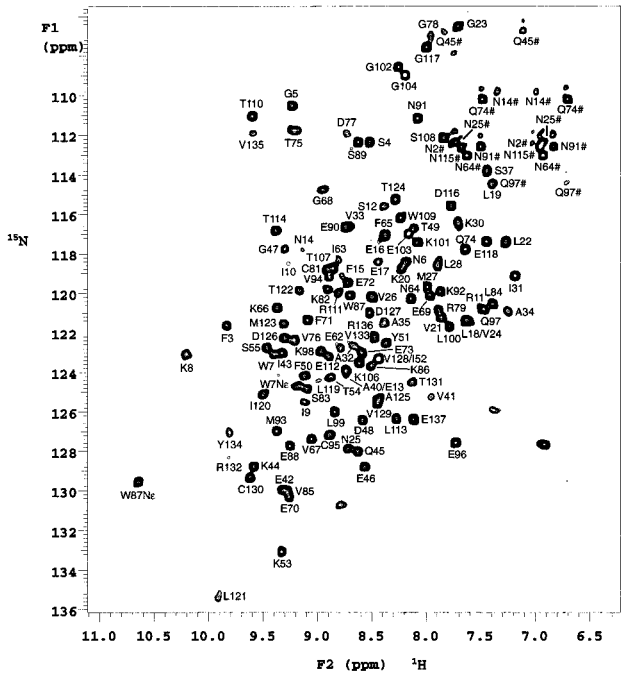

FIGURE 2: 2D $^{1}H-^{15}N$ HSQC spectrum of uniformly ^{15}N-labeled wild type apo-CRABPII recorded at a ^{1}H frequency of 600 MHz with coherence selection by pulsed field gradients and sensitivity enhancement. Sequential assignments are indicated with the one-letter amino acid code and residue number. The side chain amides of Asn and Gln are indicated by #. The unlabeled peaks are most probably from the side chains of arginines.

experiments, their sequential assignment posed a big challenge. The following residues had weak cross-peaks in the $^{1}H-^{15}N$ HSQC spectrum: Lys8−Glu17, Leu28, Lys30, Ala32−Ala35, Ala40, Val41, Thr54, Glu62, Ile63, Val76−Gly78, Leu119, Leu121, and Thr131−Val135. They were assigned by spin system identifications combined with sequential and long-range (interstrand) NOEs. Because of the excellent chemical shift dispersion of the protein, 2D homonuclear TOCSY and NOESY data (both in D_2O) were especially useful for assigning these residues. Furthermore, 46 amide protons showed cross-peaks with other protons in

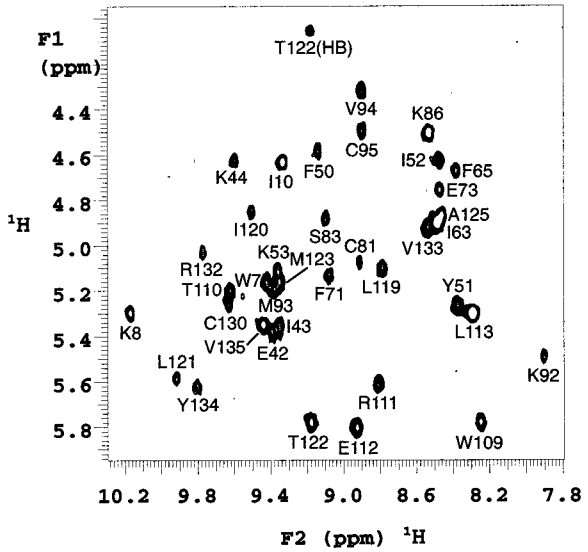

FIGURE 3: Fingerprint region of the homonuclear 2D TOCSY spectrum of apo-CRABPII recorded with a 40 ms mixing time. The TOCSY experiment was initiated more than 24 h after dissolving a lyophilized protein sample in PBS buffer (pD 7.5) in D_2O.

the 2D homonuclear spectra (Figure 3). Interestingly, the amide protons of Lys8, Ile10, Ile63, Leu119, Leu121, and Arg132−Val135 showed cross-peaks with the α-protons in the 2D homonuclear TOCSY spectrum in D_2O but had weak cross-peaks in the $^{1}H-^{15}N$ HSQC spectrum (Figure 2). The sequential assignments of many of these residues were also facilitated by comparison with the sequential assignments of the wild type holo-CRABPII (L. Wang et al., unpublished) and the apo form of the site-directed mutant R111M (L. Wang et al., unpublished). Most weak peaks in the $^{1}H-^{15}N$ HSQC spectrum of the wild type apo-CRABPII became much stronger upon the binding of RA or with the point mutation, and thus could be assigned unambiguously for holo-CRABPII and apo-R111M. Since neither the binding of RA nor the mutation changes the chemical shifts of the majority of residues, comparative analysis of NMR spectra of the three forms of CRABPII, particularly the H^N, N, H^α, and C^α resonances, helped the assignment of the weak signals of the apo-CRABPII. The resonance assignment of the leucine and valine residues was also assisted by selective labeling.

The following 11 residues were not observed in the $^{1}H-^{15}N$ HSQC spectrum: Asn2, Arg29, Ala36, Lys38, Thr56−Thr61, and Asn115. However, the spin systems of most of these residues could be identified by the analysis of the homonuclear 2D DQF-COSY, TOCSY, and 3D HCCH-TOCSY spectra. Sequential resonance assignments could be made for Asn2, Thr56, Thr57, Val58, Thr60, and Thr61 on the basis of interstrand NOEs ($d_{\alpha\alpha}$) and comparisons with NMR spectra of holo-CRABPII and apo-R111M. The resonances of Arg29, Lys38, Pro39, and Arg59 could not be assigned at present. The chemical shifts of all the assigned ^{1}H, ^{13}C, and ^{15}N resonances are listed in Table S1 of the Supporting Information.

Stereospecific Resonance Assignment. To better determine the solution structure of CRABPII, stereospecific resonance assignments were made whenever possible. β-Methylene protons were stereospecifically assigned on the basis of the

Table 1: Restraint and Structural Statistics of Apo-CRABPII

Restraint Statistics		
number of experimental NOE restraints		
intraresidue		647
sequential		560
medium-range		248
long-range		835
total		2290
number of hydrogen bonds		92
Structural Statistics	$\langle SA \rangle^a$	$\langle SA \rangle_r^b$
rmsd from experimental distance restraints (Å) (2290)	0.036 ± 0.001	0.028
deviation from idealized covalent geometry		
bonds (Å)	0.004 ± 0.001	0.003
angles (deg)	0.742 ± 0.028	0.583
impropers (deg)	0.604 ± 0.006	0.482
Measures of Structural Quality (by Procheck)		
Ramachandran plot		
residues in most favorable regions (%)	55.6 ± 2.4	54.8
residues in additional allowed regions (%)	37.1 ± 1.6	37.1
number of bad contacts	8 ± 2	8
hydrogen bond energy	0.40 ± 0.10	0.50
overall *G*-factor	-0.30 ± 0.02	−0.30
Coordinate Precision		
rmsd for the C^α trace (Å)	0.84 ± 0.21	0.47 ± 0.15^c
rmsd for backbone atoms (Å)	0.89 ± 0.25	0.54 ± 0.18^c
rmsd for all heavy atoms (Å)	1.12 ± 0.28	0.92 ± 0.20^c

[a] $\langle SA \rangle$ represents the final 25 simulated annealing structures. [b] $\langle SA \rangle_r$ is the restrained minimized mean structure obtained by restrained regularization of the mean structure, which is obtained by averaging the coordinates of the individual SA structures best fitted to each other. [c] Residues Ala32−Pro39 and Thr57−Glu62 were excluded from the rmsd calculations.

qualitative estimations of $^3J_{\alpha\beta}$ constants from the DQF-COSY spectrum in conjunction with the NOE data (*53*). The methyl groups of valine and leucine residues were stereospecifically assigned in a similar manner. Stereospecific assignments were obtained for H^β methylene protons of 43 residues and for methyl protons of six valine residues and four leucine residues.

Structure Determination. A total of 2290 structurally useful distance restraints were obtained from the analyses of the homonuclear 2D NOESY (D_2O) and 3D $^1H-^{15}N$ NOESY−HSQC spectra (Table 1). Of the NOE restraints, 835 were long-range NOEs. On average, each residue had ~17 NOE restraints, but the number of NOE restraints per residue varied greatly along the amino acid sequence (Figure 4). The residues situated in the turns or loops and the entrance region had NOE restraints well below the average. Ninety-two hydrogen bond restraints characterizing 46 hydrogen bonds were included in the structural refinements. Twenty-five structures with no NOE violations of >0.3 Å are shown in Figure 5A. The statistics of the structures are summarized in Table 1. Except for the residues from Ala32 to Pro39 and the entrance region, the structures were well-defined. If residues Ala32−Pro39 and Thr57−Glu62 were excluded, the precision of the structures (rmsd of the 25 coordinates) was 0.54 Å for the backbone atoms (N, C^α, C′, and O) and 0.92 Å for all heavy atoms.

Description of the Solution Structure of Apo-CRABPII. The solution structure of apo-CRABPII mainly consists of two nearly orthogonal antiparallel β-sheets twisted to form a flattened β-barrel (Figure 5A), a structural feature shared by all the published structures of iLBPs (*12*). While the first helix and the turn of the helix−turn−helix motif were well-defined, the segment corresponding to the second helix in the crystal structures was largely disordered because of the paucity of NOE restraints. The chemical shift indices suggest that residues 30−35 are helical (*54*). However, the chemical shift indices were not included in the NMR structure refinement. This segment of the protein, athough possibly helical, undergoes conformational changes as discussed in a later section. A partial unwinding of the second helix has been observed in the crystal structure of unliganded CRABPII mutant R111M (*55*).

As in other ILBPs, owing to a large gap, there are no main chain hydrogen bonds between βD and βE. The gap gradually widens from the N terminus to the C terminus of βD so that the two strands look like a long V-typed fork. The distances from C^α of Val76 in the βE−βF loop to the C^αs of Val58 in the βC−βD loop and Val24 in the loop linked to the first helix are 20.7 and 17.0 Å, respectively. The entrance to the barrel is wide open and readily accessible to RA (Figure 6).

Comparisons with the Crystal Structures of Holo-CARBPII and Apo-CRABPI. Figure 5B shows the overlay of the C^α traces of the restrained minimized mean structure of the apo-CRABPII and the crystal structure of holo-CRABPII. The structure can be superimposed with C^α deviations of 3.52, 2.04, and 1.65 Å for all residues, the regular secondary structures, and all residues excluding Val24−Ser37, Glu74−Pro80, and Leu100−Gly104, respectively. The main differences between the two structures are located in the regions around the ligand entrance. The second helix is well-defined in the crystal structure of the holoprotein but appears to be flexible in the apo form in solution, especially the C-terminal half. The βC−βD loop moves away from the main body of the protein by ~5 Å in the solution structure of the apoprotein. The C-terminal half of βE and the N-terminal half of βF in the solution structure of the apoprotein do not twist toward the center of the protein to constrict the ligand entrance as they do in the crystal structure of the holoprotein. Consequently, the long loop between βG and βH also moves away from the main body of the apoprotein. The distance between C^α of Val76 in the βE−βF loop and C^α of Val58 in the βC−βD loop is ~8.0 Å longer in the solution structure of the apoprotein than in the crystal structure of the holoprotein. The distance between C^α of Val76 and C^α of Val24 in the βA−βB loop is ~6.7 Å longer in the solution structure of the apoprotein than in the crystal structure of the holoprotein. As a result, the ligand entrance in the solution structure of the apoprotein is greatly enlarged with a much more exposed binding pocket (Figure 6). In particular, residues Val24, Leu28, Ile31, Val58, Arg59, and Val76 move away from each other so that the side chains of Arg111, Arg132, and Tyr134 that interact with the carboxyl group of RA are easily accessible to the ligand. However, the relative positions of Arg111, Arg132, and Tyr134 are quite similar to those observed in the crystal structure of holo-CRABPII in that the backbone atoms of these residues can be superimposed rather well.

In comparison to other parts of the protein, which are well-defined, the ligand entrance region of the solution structure

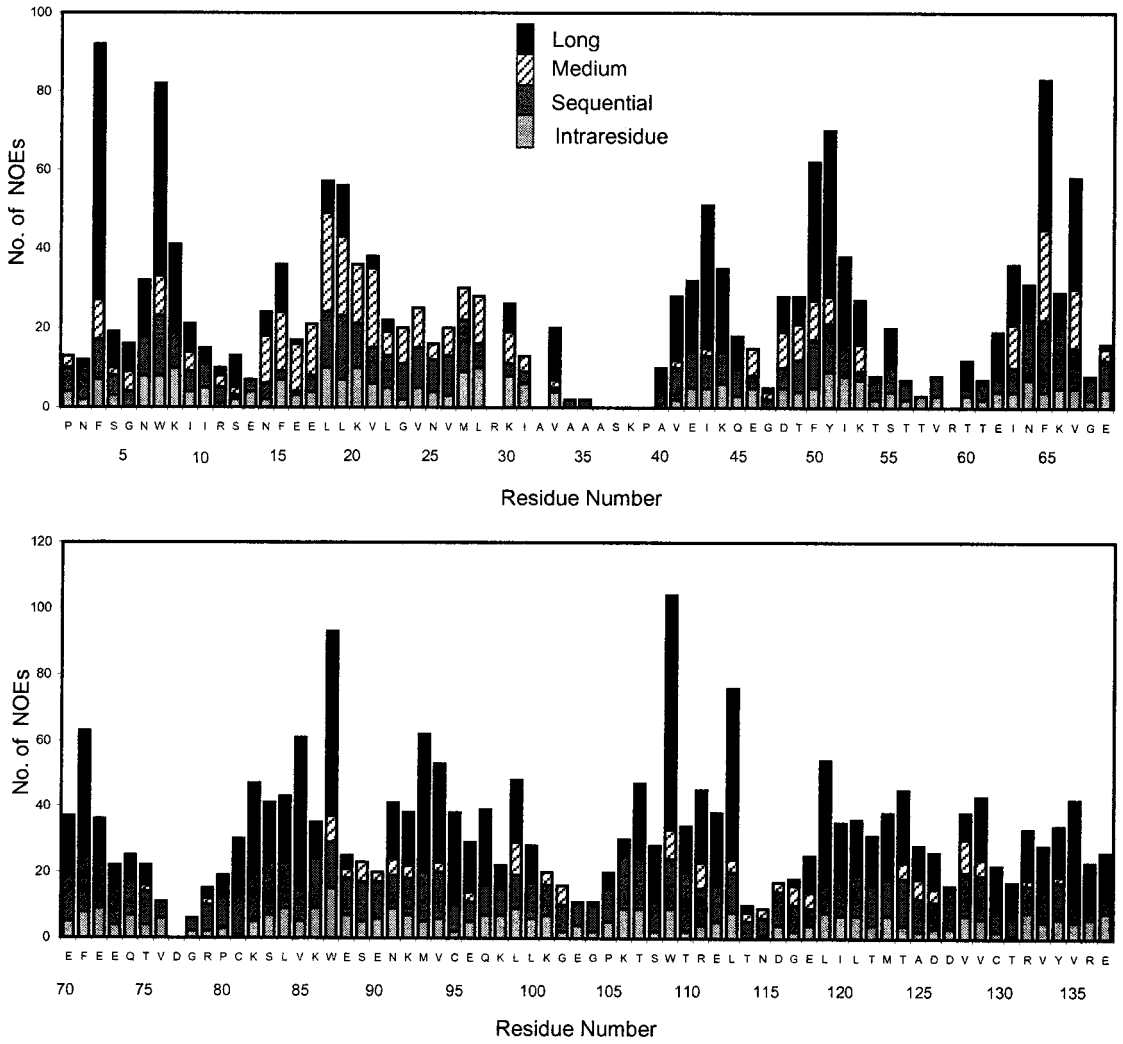

FIGURE 4: Distribution of NOEs along the amino acid sequence of CRABPII. For intraresidue NOEs, only those that are structurally useful were included.

of apo-CRABPII appears to be disordered. Most residues in the region have weak or no observable peaks in all ^{15}N-edited spectra. The number of the experimental distance restraints per residue for the region is well below the average. However, except for Ala32−Pro39, the differences between the solution structure of the apoprotein and the crystal structure of the holoprotein (Figure 5B) are larger than between any two conformations from the ensemble of 25 refined NMR solution conformations (Figure 5A). Thus, the differences between the solution structure of the apoprotein and the crystal structure of the holoprotein are real.

Most of the differences between the solution structure of the apo-CRABPII and the crystal structure of holo-CRABPII are also observed between the solution structure of apo-CRABPII and the crystal structure of apo-CRABPI (*14*) (Figure 5C).

Dynamical Properties. As detailed earlier, about one-quarter of the residues showed weak or no signals in the 2D ^{1}H−^{15}N HSQC spectrum (Figure 2). Some of them were situated in the turns or loops between elements of regular secondary structure. Surprisingly, many others assumed regular α-helical or β-sheet structures. Only the residues in the βC−βD loop and the βE−βF loop and Asn115 in the βH−βI loop showed weak or no cross-peaks in the ^{1}H−^{15}N HSQC spectrum. The residues in the longest loop between βG and βH showed the highest intensities in the ^{1}H−^{15}N HSQC spectrum. By contrast, residues in the long loop of holo-CRABPII had high temperature factors in the X-ray structure. Interestingly, most of these residues that showed weak or no cross-peaks in the ^{1}H−^{15}N HSQC spectrum are located in the RA-binding pocket (Figure 7). Among the 21 residues that constitute the RA-binding pocket (*13*), 16 residues exhibited weak or no detectable cross-peaks in the ^{1}H−^{15}N HSQC spectrum.

It is unlikely that water saturation was the cause for the diminution or disappearance of the several cross-peaks that are missing from the ^{1}H−^{15}N HSQC spectrum. The spectrum was recorded with a "water flip-back" pulse sequence designed to minimize water saturation and dephasing (*31*, *56*). Furthermore, for several weak or missing HSQC peaks, the amide protons remained 2 days after the lyophilized protein was dissolved in D_2O and showed cross-peaks in the fingerprint regions of the homonuclear 2D spectra recorded in D_2O (Figure 3), indicating that these amide protons exchange slowly with solvent and should not be perturbed by water saturation. The most likely cause for the weak or missing HSQC peaks was line broadening resulting from conformational exchange and/or hydrogen exchange with solvent. For Lys8, Ile10, Leu19, Leu121, and Arg132−Val135, clearly, the weak peaks were due to line broadening

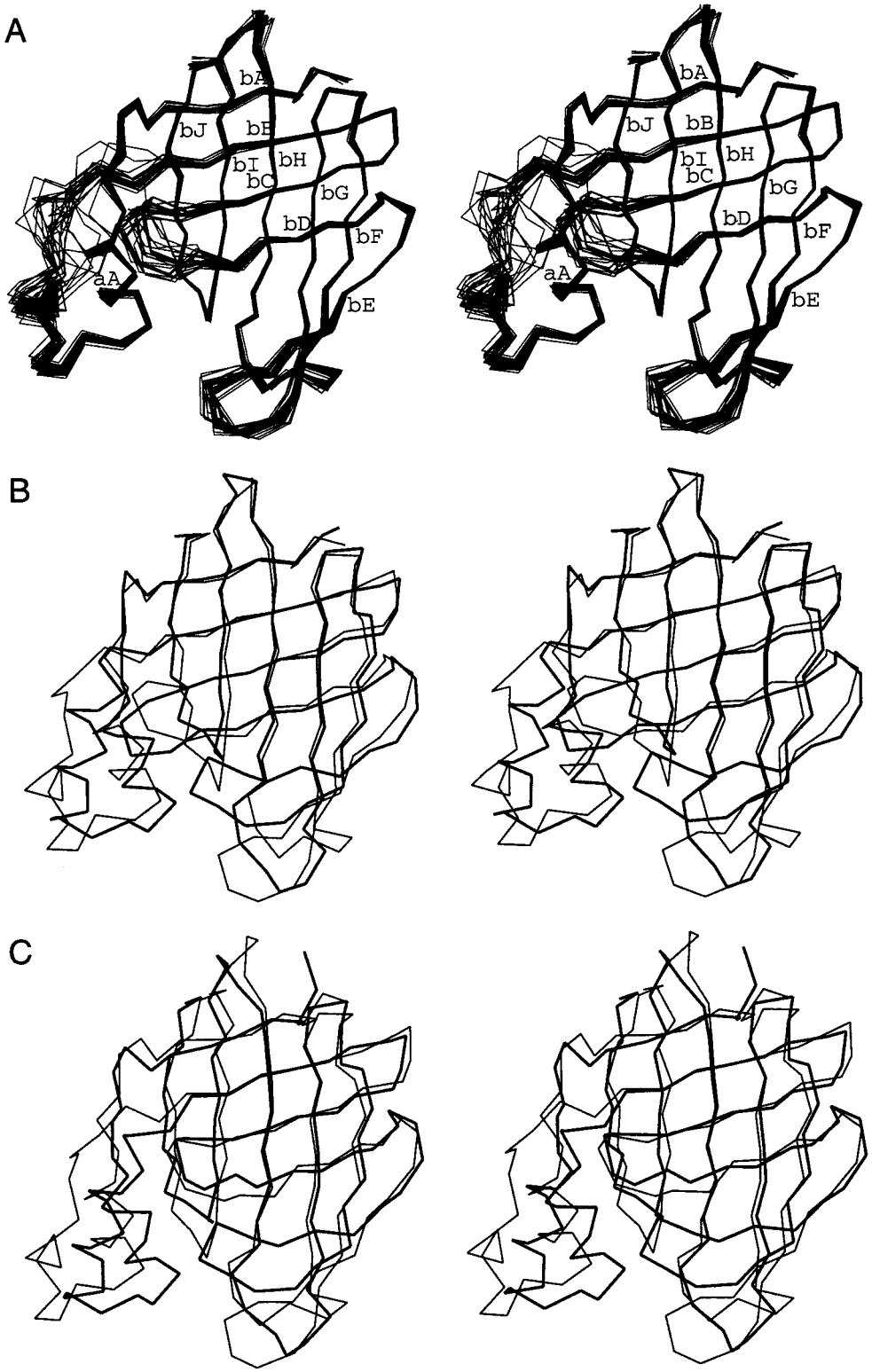

FIGURE 5: (A) Stereoview of the C^{α} traces of the superimposed 25 final refined solution structures of apo-CRABPII. (B) Stereoview of the C^{α} trace of the restrained minimized mean structure of apo-CRABAPII (thin line) superimposed with the C^{α} trace of the crystal structure of holo-CRABAPII (thick line). (C) Stereoview of the C^{α} trace of the restrained minimized mean structure of apo-CRABAPII (thin line) superimposed with the C^{α} trace of the crystal structure of apo-CRABAPI (molecule A) (thick line).

of their nitrogen resonances since their amide protons exhibited sharp signals and showed cross-peaks with α-protons in 2D homonulcear spectra recorded in D_2O (Figure 3). The line broadening of the nitrogen resonances was in turn due to conformational exchange at rates that are intermediate on the NMR time scale. The clustering of the weak or missing peaks suggested that most of the rest of the residues may also experience conformational exchange. Hydrogen exchange could also contribute to the diminishing or disappearing of the HSQC peaks for these residues because their backbone amide exchanged with solvent more rapidly and did not show cross-peaks in 2D homonulcear spectra recorded in D_2O. However, it may be difficult to dissect the relative contributions of the two exchange

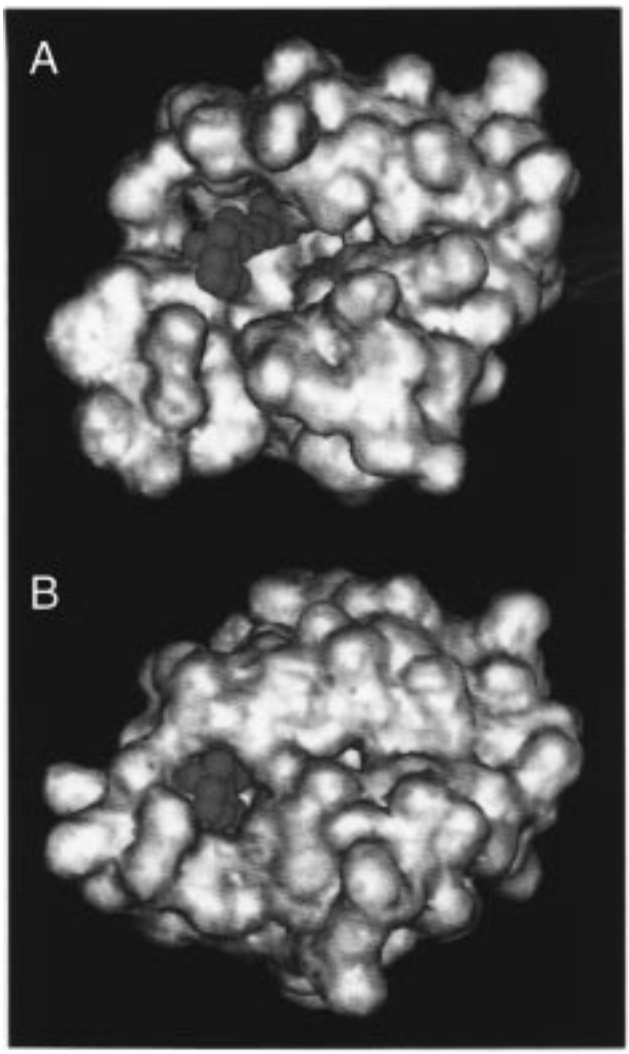

FIGURE 6: Solvent-accessible surfaces of apo-CRABPII (A) and holo-CRABPII (B). The illustration for holo-CRABPII was derived from the crystal coordinates of holo-CRABPII (*13*). RA (green) in panel A is positioned on the basis of the superposition of the solution structure of apo-CRABPII and the crystal structure of holo-CRABPII. It is shown as a reference for the accessibility of the ligand binding pocket. The figure was prepared with the program Insight II (MSI).

processes because the weak or missing HSQC peaks will make it difficult to measure the hydrogen exchange rates or relaxation parameters of backbone amides for these residues. The upper limits of the hydrogen exchange rates, nevertheless, may be calculated on the basis of the CRABPII sequence using the formula and parameters developed and calibrated by Englander and colleagues (*57*) with random coil peptides. The calculated hydrogen exchange rates ranged from 3.6 to 160 s^{-1} with a mean of 32 s^{-1}. Only Ser12, Asn115, and Thr131 had exchange rates higher than their $^1J_{NH}$ coupling constants (~95 Hz). The hydrogen exchange rates in native CRABPII are expected to be significantly slower than 95 s^{-1} for most of the residues. Thus, the effect of amide hydrogen exchange on their peak intensities is probably minor. Even if the exchange rates are close to those calculated on the basis of the unfolded CRABPII sequence and therefore hydrogen exchange has a significant effect on their peak intensities, the fast hydrogen exchange is likely due to rapid conformational exchange.

A slow conformational exchange with a lifetime of at least 40 ms was observed in our previous studies, resulting in two sets of cross-peaks for Trp87 (*8*). It was noted that Trp87 is located at N terminus of βF far away from the RA-binding pocket. The residues in the RA-binding pocket likely undergo intermediate or fast conformational exchange because only one set of NMR signals was observed for these residues. The clustering of the mobile residues around the RA-binding pocket suggests that the RA-binding pocket may undergo collective motions in the absence of the RA ligand.

A flexible RA-binding pocket is consistent with biochemical and NMR studies of CRABPI. Limited proteolysis showed that helix α2 of CRABPI is significantly more susceptible to proteolysis in the apo form than in the holo form (*58*), suggesting that RA binding induces a conformational change or that helix α2 is more mobile in the apo form. Hydrogen exchange measurements revealed that helix α2 and the βC−βD loop of CRABPI have much higher exchange rates in the apo form than in the holo form (*15*), indicating that these parts of the molecule are more mobile in the apo form. Other iLBPs also have been found to exhibit similar dynamical properties. For example, it was shown by NMR that the second helix of rat intestinal fatty acid binding protein is disordered in solution (*59*, *60*). In the case of bovine heart fatty acid binding protein, up to four sets of proton resonances were observed for Ser22−Thr36 in the helix−turn−helix motif, Thr53−Thr60 in the βC−βD loop, and His119−Ala122 in the βI−βJ loop, indicating these residues have two or more slowly exchanging conformations in solution (*61*).

Is CRABPII Dimeric in Solution? Unlike other iLBPs, apo-CRABPI was crystallized in a dimeric form (*14*). The crystalline dimer is held together by an intermolecular β-sheet formed by the βD strands of two CRABPI molecules, resulting in a 20-stranded double β-barrel with slightly more open RA-binding pockets. It was suggested that dimerization may be the mechanism by which CRABPI opens the ligand entrance so that RA can enter or exit the binding pocket without steric hindrance. In light of the potential significance of the dimerization to the ligand entrance problem, we carefully examined the possibility of the formation of the intermolecular β-sheet. We concluded that apo-CRABPII is predominately monomeric in solution for the following reasons. (i) The elution volume of apo-CRAPBII on a Sephadex G-50 gel-filtration column was characteristic of a monomer. (ii) For the most part, the line widths of the NMR signals of CRABPII were consistent with a monomeric structure. (iii) Only NOEs characteristic of a monomer were observed. For example, according to the dimeric crystal structure of apo-CRABPI, the distance between H^{α} of Thr61 of molecule A and H^{β} of Thr60 of molecule B is 2.5 Å but the distance between H^{α} of Thr61 and H^{β} of Thr60 of the same molecule is 5.9 Å. Thus, a cross-peak between these two atoms should be observed for a stable dimer but not for a monomer. Although signals from these two protons were detected and assigned, no NOE cross-peak between the two was detected. Although the formation of transient dimers could not be ruled out, the transient dimers, if they exist, can only be a minor population under the conditions of the NMR or gel-filtration experiments. What is the likelihood of the dimerization in vivo? Since the cellular concentration of CRABPII is much lower than the concentrations of the

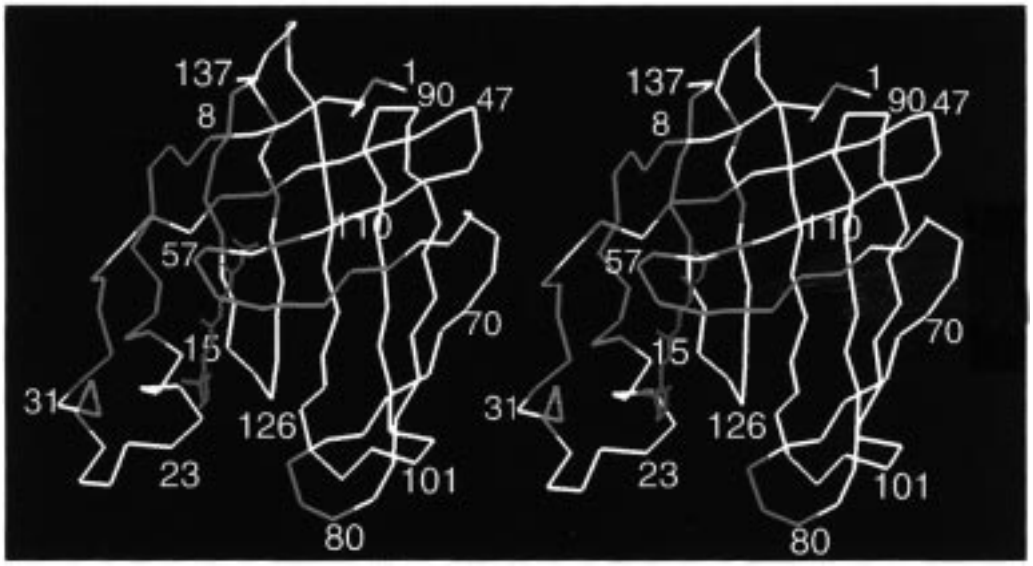

FIGURE 7: Relative peak intensities of the 2D $^{1}H-^{15}N$ HSQC spectrum of apo-CRABPII color-coded along the C^{α} trace of the solution structure. The strong peaks are white, the weak peaks pink, and the missing peaks cyan. RA is positioned on the basis of the superposition of the solution structure of apo-CRABPII and the crystal structure of holo-CRABPII.

NMR samples, the concentration of dimeric species would be even lower in vivo.

Implications for RA Binding. The crystal structures of holo-CRABPI and CRABPII suggested that RA cannot enter or exit the ligand binding pockets of the proteins in the absence of significant conformational changes. On the basis of limited proteolysis of several intracellular lipid binding proteins, including CRABPI, Jamison and co-workers proposed that a rigid body movement of the helix−turn−helix motif may serve as the mechanism by which the family of proteins opens their ligand binding pockets (*58*). In light of the solution structure of apo-CRABPII, it is unlikely that the two helices move as rigid rods as previously proposed. Rather, the second helix of the helix−turn−helix motif is flexible and undergoes conformational exchange. The dynamic nature of the second helix may be the cause of its high susceptibility to proteolysis.

On the basis of comparison of the crystal structures of apo- and holo-CRABPI, Thompson and co-workers suggested that movement of the $\beta C-\beta D$ loop is responsible for the opening of the ligand entrance (*14*). Furthermore, as mentioned above, it has been proposed that movement of the $\beta C-\beta D$ loop is dependent on formation of the intermolecular β-sheet. Comparison of the solution structure of apo-CRABPII and the crystal structure of holo-CRABPII confirms the hypothesis that the $\beta C-\beta D$ loop moves when RA is bound. However, the movement of the $\beta C-\beta D$ loop that opens the binding pocket is shown by NMR not to involve dimerization of the protein because CRABPII is predominately monomeric in solution.

The results reported here demonstrate that the ligand entrance of monomeric apo-CRABPII in solution is wide open and readily accessible to retinoic acid. Comparison of the solution structure of apo-CRABPII with the crystal structure of holo-CRABPII suggests that the conformational change responsible for opening the ligand entrance can be explained as a concerted movement of three structural elements, namely, the second helix, the $\beta C-\beta D$ loop, and the $\beta E-\beta F$ loop. The partial unwinding of the second helix and the movements of the $\beta C-\beta D$ and the $\beta E-\beta F$ loops have also been observed in the crystal structure of the apo-CRABPII mutant R111M, albeit with smaller magnitudes (*55*). A widely opened entrance may be essential for binding of RA, because RA is a long, relatively rigid, negatively charged molecule. A narrow entrance lined with the hydrophobic side chains would result in unfavorable interactions with RA. The entry of RA into the deep binding pocket may be further facilitated by the positively charged potentials generated by Arg29, Arg59, Arg111, and Arg132 (*55*). Binding of RA induces significant conformational changes in CRABPII. Furthermore, the interactions between RA and CRABPII may stabilize the structural elements constituting the RA-binding pocket, especially the second helix, the $\beta C-\beta D$ loop, and the $\beta E-\beta F$ loop.

Conclusions. Using multidimensional NMR spectroscopy, we have determined the first solution structure of a CRABP. Comparison of the solution structure of apo-CRABPII with the crystal structure of holo-CRABPII indicates that the largest conformational differences between the two structures are localized at the ligand entrance. The ligand entrance of apo-CRABPII is greatly enlarged and readily accessible to RA, mainly due to a concerted movement of the second helix and the $\beta C-\beta D$ and $\beta E-\beta D$ loops. Furthermore, the ligand binding pocket of apo-CRABPII is flexible as indicated by analysis of the cross-peak intensities of the $^{1}H-^{15}N$ HSQC spectrum. CRABPII is predominately monomeric in solution as determined from NMR and biochemical evidence. Although the formation of transient dimers could not be ruled out, dimerization apparently is not a prerequisite for entry of RA into the ligand binding pocket of CRABPII.

SUPPORTING INFORMATION AVAILABLE

A table listing the ^{1}H, ^{15}N, and ^{13}C assignments of apo-CRABPII at pH 7.3 and 25 °C (3 pages). Ordering information is given on any current masthead page.

REFERENCES

1. Napoli, J. L. (1996) *FASEB J. 10*, 993−1001.

2. Lampron, C., Rochette Egly, C., Gorry, P., Dolle, P., Mark, M., Lufkin, T., LeMeur, M., and Chambon, P. (1995) *Development 121*, 539−48.
3. Fawcett, D., Pasceri, P., Fraser, R., Colbert, M., Rossant, J., and Giguere, V. (1995) *Development 121*, 671−9.
4. Åström, A., Tavakkol, A., Pettersson, U., Cromie, M., Elder, J. T., and Voorhees, J. J. (1991) *J. Biol. Chem. 266*, 17662−6.
5. Newcomer, M. E. (1995) *FASEB J. 9*, 229−39.
6. Fiorella, P. D., and Napoli, J. L. (1991) *J. Biol. Chem. 266*, 16572−9.
7. Fiorella, P. D., Giguere, V., and Napoli, J. L. (1993) *J. Biol. Chem. 268*, 21545−52.
8. Wang, L., Li, Y., and Yan, H. (1997) *J. Biol. Chem. 272*, 1541−7.
9. Bucco, R. A., Zheng, W. L., Davis, J. T., Sierra Rivera, E., Osteen, K. G., Chaudhary, A. K., and Ong, D. E. (1997) *Biochemistry 36*, 4009−14.
10. Jing, Y., Waxman, S., and Mira-y-Lopez, R. (1997) *Cancer Res. 57*, 1668−72.
11. Boylan, J. F., and Gudas, L. J. (1991) *J. Cell Biol. 112*, 965−79.
12. Banaszak, L., Winter, N., Xu, Z., Bernlohr, D. A., Cowan, S., and Jones, T. A. (1994) *Adv. Protein Chem. 45*, 89−151.
13. Kleywegt, G. J., Bergfors, T., Senn, H., Le Motte, P., Gsell, B., Shudo, K., and Jones, T. A. (1994) *Structure 2*, 1241−58.
14. Thompson, J. R., Bratt, J. M., and Banaszak, L. J. (1995) *J. Mol. Biol. 252*, 433−46.
15. Rizo, J., Liu, Z. P., and Gierasch, L. M. (1994) *J. Biomol. NMR 4*, 741−60.
16. Muchmore, D. C., McIntosh, L. P., Russell, C. B., Anderson, D. E., and Dahluist, F. W. (1989) *Methods Enzymol. 177*, 44−73.
17. States, D. J., Haberkorn, R. A., and Ruben, D. J. (1982) *J. Magn. Reson. 48*, 286−92.
18. Marion, D., Ikura, M., Tschudin, R., and Bax, A. (1989) *J. Magn. Reson. 85*, 393−9.
19. Piantini, U., Sørensen, O. W., and Ernst, R. R. (1982) *J. Am. Chem. Soc. 104*, 6800−1.
20. Rance, M., Sørensen, O. W., Bodenhausen, G., Wagner, G., Ernst, R. R., and Wüthrich, K. (1983) *Biochem. Biophys. Res. Commun. 117*, 479−85.
21. Braunschweiler, L., and Ernst, R. R. (1983) *J. Magn. Reson. 53*, 521−8.
22. Bax, A., and Davis, D. G. (1985) *J. Magn. Reson. 65*, 355−60.
23. Griesinger, C., Otting, G., Wüthrich, K., and Ernst, R. P. (1988) *J. Am. Chem. Soc. 110*, 7870−2.
24. Jeener, J., Meier, B. H., Bachmann, P., and Ernst, R. R. (1979) *J. Chem. Phys. 71*, 4546−53.
25. Macura, S., and Ernst, R. R. (1980) *Mol. Phys. 41*, 95−117.
26. Smallcombe, S. H. (1993) *J. Am. Chem. Soc. 115*, 4776−85.
27. Bodenhausen, G., and Ruben, D. J. (1980) *Chem. Phys. Lett. 69*, 185−8.
28. Kay, L. E., Keifer, P., and Saarinen, T. (1992) *J. Am. Chem. Soc. 114*, 10663−5.
29. Fesik, S. W., and Zuiderweg, E. R. P. (1988) *J. Magn. Reson. 78*, 588−93.
30. Marion, D., Driscoll, P. C., Kay, L. E., Wingfield, P. T., Bax, A., Gronenborn, A. M., and Clore, G. M. (1989) *Biochemistry 28*, 6150−6.
31. Zhang, O., Kay, L. E., Olivier, J. P., and Forman Kay, J. D. (1994) *J. Biomol. NMR 4*, 845−58.
32. Kay, L. E., Ikura, M., Tschudin, R., and Bax, A. (1990) *J. Magn. Reson. 89*, 496−514.
33. Grzesiek, S., and Bax, A. (1992) *J. Magn. Reson. 96*, 432−40.
34. Bax, A., and Ikura, M. (1991) *J. Biomol. NMR 1*, 99−104.
35. Wittekind, M., and Mueller, L. (1993) *J. Magn. Reson., Ser. B 101*, 201−5.
36. Muhandiram, D. R., and Kay, L. E. (1994) *J. Magn. Reson., Ser. B 103*, 203−16.
37. Grzesiek, S., and Bax, A. (1992) *J. Am. Chem. Soc. 114*, 6291−3.
38. Grzesiek, S., Anglister, J., and Bax, A. (1993) *J. Magn. Reson. 101*, 114−9.
39. Bax, A., Clore, G. M., and Gronenborn, A. M. (1990) *J. Magn. Reson. 88*, 425−31.
40. Kay, L. E., Xu, G.-Y., Singer, A. U., Muhandiram, D. R., and Forman-Kay, J. D. (1993) *J. Magn. Reson., Ser. B 101*, 333−7.
41. Shaka, A. J., Barker, P. B., and Freeman, R. (1985) *J. Magn. Reson. 64*, 547−52.
42. Shaka, A. J., Lee, C. J., and Pines, A. (1988) *J. Magn. Reson. 77*, 274−93.
43. Shaka, A. J., Keeler, J., Frenkiel, T., and Freeman, R. (1983) *J. Magn. Reson. 52*, 335−8.
44. McCoy, M. A., and Mueller, L. (1992) *J. Am. Chem. Soc. 114*, 2108−12.
45. Zhu, G., and Bax, A. (1992) *J. Magn. Reson. 100*, 202−7.
46. Marion, D., Ikura, M., and Bax, A. (1989) *J. Magn. Reson. 84*, 425−30.
47. Wüthrich, K., Billeter, M., and Braun, W. (1983) *J. Mol. Biol. 169*, 949−61.
48. Nilges, M., Gronenborn, A. M., and Clore, G. M. (1988) *FEBS Lett. 229*, 317−24.
49. Brünger, A. T. (1992) *X-PLOR Version 3.1: A System for Crystallography and NMR*, Yale Univeristy Press, New Haven, CT.
50. Brooks, B. R., Bruccoleri, R. E., Olafson, B. D., States, D. J., and Karplus, M. (1983) *J. Comput. Chem. 4*, 187−217.
51. Laskowski, R. A., MacArthur, M. W., Moss, D. S., and Thornton, J. M. (1993) *J. Appl. Crystallogr. 26*, 283−91.
52. Laskowski, R. A., Rullmannn, J. A., MacArthur, M. W., Kaptein, R., and Thornton, J. M. (1997) *J. Biomol. NMR 8*, 477−86.
53. Basus, V. J. (1989) *Methods Enzymol. 177*, 132−49.
54. Wishart, D. S., and Sykes, B. D. (1994) *Methods Enzymol. 239*, 363−92.
55. Chen, X., Tordova, M., Gilliland, G. L., Wang, L., Li, Y., Yan, H., and Ji, X. (1998) *J. Mol. Biol. 278*, 641−53.
56. Grzesiek, S., and Bax, A. (1993) *J. Am. Chem. Soc. 115*, 12593−4.
57. Bai, Y., Milne, J. S., Mayne, L., and Englander, S. W. (1993) *Proteins 17*, 75−86.
58. Jamison, R. S., Newcomer, M. E., and Ong, D. E. (1994) *Biochemistry 33*, 2873−9.
59. Hodsdon, M. E., and Cistola, D. P. (1997) *Biochemistry 36*, 2278−90.
60. Hodsdon, M. E., and Cistola, D. P. (1997) *Biochemistry 36*, 1450−60.
61. Lücke, C., Lassen, D., Kreienkamp, H. J., Spener, F., and Rüterjans, H. (1992) *Eur. J. Biochem. 210*, 901−10.

BI9808924